Fractal energy carpets in non-Hermitian Hofstadter quantum mechanics

Maxim N. Chernodub*
CNRS, Laboratoire de Mathématiques et Physique Théorique, UMR 7350, Université de Tours, 37200 Tours, France;
Department of Physics and Astronomy, University of Gent, Krijgslaan 281, S9, B-9000 Gent, Belgium;
and Soft Matter Physics Laboratory, Far Eastern Federal University, Sukhanova str., 8, Vladivostok 690950, Russia

Stéphane Ouvry†
CNRS, Laboratoire de Physique Théorique et Modèles Statistiques, UMR 8626, Université Paris-Sud, 91405 Orsay, France
(Received 17 April 2015; published 5 October 2015)

We study the non-Hermitian Hofstadter dynamics of a quantum particle with biased motion on a square lattice in the background of a magnetic field. We show that in quasimomentum space, the energy spectrum is an overlap of infinitely many inequivalent fractals. The energy levels in each fractal are space-filling curves with Hausdorff dimension 2. The band structure of the spectrum is similar to a fractal spider web in contrast to the Hofstadter butterfly for unbiased motion.

DOI: 10.1103/PhysRevE.92.042102 PACS number(s): 05.50.+q, 04.60.Nc, 71.70.Di, 05.40.Fb

I. INTRODUCTION

It is well known that the energy spectrum of an electrically charged particle moving in the background of an external magnetic magnetic field on a two-dimensional infinite square lattice has a beautiful fractal structure known as the Hofstadter butterfly [1]. The energy bands plotted against the magnetic flux reveal a complex pattern that resembles a butterfly, hence the name. The fractality of the Hofstadter butterfly is revealed in the fact that small regions of the energy spectrum contain a distorted copy of a larger region, thus exhibiting the self-similarity property at all scales. This property is a characteristic feature of a fractal [2].

The Hofstadter spectrum was originally obtained in a tight-binding model that describes the motion on a square lattice of a (spinless) charged particle hopping from one site to one of the nearest sites in the presence of an external magnetic field perpendicular to the lattice plane.

In this paper, we address the problem of a *biased* quantum motion where the motion is constrained—"biased"—by the condition that the hopping of the particle to the left is now forbidden, while it can still freely hop to the other nearest sites (right, up, and down) as indicated in Fig. 1. The particle is electrically charged so that its motion is affected by the presence of the magnetic field. Its dynamic is described by a truncated non-Hermitian Hofstadter Hamiltonian.

This quantum system was introduced in Ref. [3], where its relation with biased classical random walks—i.e., random walks on a square lattice conditioned to move horizontally only to the right, never to the left [4]—was studied. Explicit trace identities relating, on the one hand, the generating functions of the algebraic area probability distribution of biased random walks to, on the other hand, the traces of powers of the quantum truncated Hamiltonian, were proposed in the so-called commensurate case in which the (normalized) magnetic flux per unit cell is a rational number. An exact solution for the quantum spectrum was derived. It turns out that the energy levels depend on two quantum numbers k_x and k_y. The quasimomentum k_y takes continuous values in $[-\pi,\pi]$ and corresponds to the plane-wave Bloch states propagating along the vertical axis, while the other quantum number k_x takes discrete values in the same interval $[-\pi,\pi]$ and fixes the boundary condition on the horizontal axis.

Following the approach of Ref. [1], where the fractal structure of the Hofstadter band spectrum is revealed when it is plotted as a function of the external magnetic flux, we are going to show below that the energy bands of the biased quantum model also exhibit, not surprisingly, a self-similar structure in the same "energy-flux" plane. In addition, we will also argue that energy levels for different magnetic fluxes reveal—when they are plotted as a function of k_y—unusual fractal patterns ("fractal carpets") in the "energy-quasimomentum" plane.

The paper is organized as follows: In Sec. II we consider the non-Hermitian Hofstadter model and its real-valued energy spectrum. In Sec. III we argue visually and numerically that the spectrum possesses a fractal structure not only for the energy bands plotted against the magnetic flux but also for the energy levels plotted against the quasimomentum k_y. An analytical argument based on Chebyshev nesting is presented in Sec. IV. It is followed by yet another analytical argument for the flattened energy bands in Sec. V. Complex-valued branches of the energy spectrum are briefly discussed in Sec. VI. The final section is devoted to our conclusions.

II. THE MODEL AND ITS SPECTRUM

A. The biased quantum model

The biased quantum non-Hermitian Hamiltonian is

$$H_\beta = T_x + T_y + T_y^{-1}, \tag{1}$$

where the operators T_x and T_y describe the hopping of the particle along (the positive directions of) the axes x and y, respectively. Quantum mechanically, the hopping operators act on a state $\Psi_{m,n}$ at lattice site (m,n) as [8]

$$\begin{aligned} T_x \Psi_{m,n} &= \Psi_{m+1,n}, \\ T_y \Psi_{m,n} &= e^{i2\pi m\beta} \Psi_{m,n+1}, \end{aligned} \tag{2}$$

*maxim.chernodub@lmpt.univ-tours.fr
†stephane.ouvry@u-psud.fr

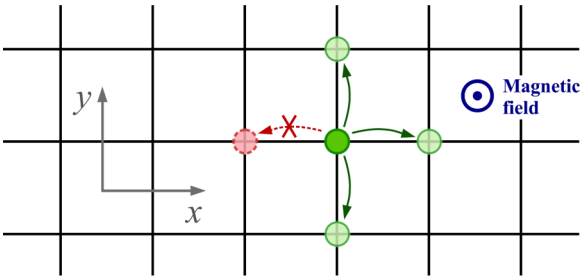

FIG. 1. (Color online) Biased motion in a magnetic field.

where[1]

$$\beta = \frac{\Phi}{\Phi_0} \tag{3}$$

is the flux Φ piercing an elementary plaquette of the square lattice counted in units of the elementary flux quantum $\Phi_0 = hc/e$. The hopping operators obey the commutation relation

$$T_x T_y = e^{-2\pi i\beta} T_y T_x. \tag{4}$$

The absence of the T_x^{-1} operator in Eq. (1)—corresponding to the absence of the hops to the left according to Fig. 1—makes the Hamiltonian H_β non-Hermitian because $T_i^\dagger \equiv T_i^{-1}$ for $i = x,y$ and, consequently, $H_\beta^\dagger \neq H_\beta$.

The normalized magnetic flux β enters only via Eqs. (2) and (4). Thus, the energy spectrum is periodic with respect to the integer shifts, $\beta \to \beta + 1$. By periodicity, we take β in the interval $[0,1]$.

B. The energy spectrum

1. General solution

In Ref. [3], the spectrum of the Hamiltonian (1) was derived in the commensurate case where the magnetic flux (3) is a rational number,

$$\beta = \frac{p}{q}, \tag{5}$$

with p and q naturally relative prime integers, so that their greatest common divisor is equal to unity,

$$\gcd(p,q) = 1. \tag{6}$$

The spectrum is obtained by solving

$$P_{p,q}(E,k_y) = e^{iqk_x}, \tag{7}$$

where

$$P_{p,q}(E,k_y) = \prod_{r=1}^{q}\left[E - 2\cos\left(k_y + 2\pi\frac{p}{q}r\right)\right] \tag{8}$$

is a degree q polynomial of the energy E. Solutions of Eqs. (7) and (8) determine the possible energies where the continuous variables $k_x \in [-\pi,\pi]$ and $k_y \in [-\pi,\pi]$ play the role of quasimomenta, and the magnetic flux β enters in Eq. (5) via the integers p and q, which label distinct energy branches.

[1]Here we use the notations of Ref. [1]. In the notations of Ref. [3], $\gamma = 2\pi\beta$ has been used instead.

The spectrum consists of the q eigenenergies

$$E_{q,r}(k_y) = 2\cos\left[\frac{1}{q}\left(\arccos\left[\cos(qk_y) + \frac{e^{iqk_x}}{2}\right] + 2\pi r\right)\right], \tag{9}$$

where $r = 1,2,\ldots,q$ maps different branches of the solutions. It includes, in general, complex valued energies that correspond either to formal instabilities or to a dissipative motion of the particle. It turns out that the spectrum is real for at least certain intervals of the quasimomentum k_y if and only if k_x is such that

$$e^{iqk_x} = \pm 1, \tag{10}$$

which corresponds to periodic $e^{iqk_x} = 1$ (antiperiodic $e^{iqk_x} = -1$) boundary conditions along the q-site-long lattice cell in the x direction. Below, we restrict ourselves to periodic and antiperiodic boundary conditions for which real eigenenergies do exist.

An interesting feature of the spectrum is that it is independent of the integer p provided p and q are relative prime integers as specified in Eq. (6).

2. Examples and symmetries of the spectrum

In Fig. 2 (top and bottom) for $q = 7$ and 8, respectively, the real energy levels are plotted as a function of k_y both for periodic (antiperiodic) boundary conditions [solid (dashed) lines]. One sees that the q real branches labeled by $r = 1,2,\ldots,q$ in Eq. (9) do materialize for particular intervals of k_y.

Since the features of Fig. 2 are generic for odd and even q, we describe them in detail below.

For odd q, the highest (lowest) real energy level is a continuous curve [solid (dashed)] for the whole quasimomentum interval $k_y \in [-\pi,\pi]$. The other $q-1$ branches are real only in q distinct k_y intervals (here we use the fact that the spectrum lies on a circle, thus the quasimomenta $k_y = -\pi$ and π are identified). These $q-1$ energy branches are grouped pairwise to form $(q-1)/2$ distorted ovals in each of these intervals. Thus, both in the periodic and antiperiodic cases, one has one continuous energy band and $q(q-1)/2$ distorted energy ovals [see in Fig. 2 (top) the 21 energy dashed (solid) ovals for $q = 7$].

The odd-q energy spectrum has a number of symmetries that are manifest in Fig. 2 (top):

$$\begin{aligned} E_{q,r}^{(\pm)}(k_y)\Big|_{q\in\text{odd}} &= E_{q,r}^{(\pm)}(-k_y) = E_{q,r}^{(\pm)}\left(k_y + \frac{2\pi n}{q}\right) \\ &= -E_{q,r}^{(\mp)}\left(k_y + \frac{(2n+1)\pi}{q}\right), \end{aligned} \tag{11}$$

with $n \in \mathbb{Z}$. Indeed, the spectrum is symmetric under both mirroring in the quasimomentum direction, $k_y \to -k_y$, and the discrete shifts $k_y \to k_y + 2\pi n/q$. Moreover, for odd q, the periodic and antiperiodic spectra are related to each other by the mirroring transformation in the energy direction $E \to -E$ and a simultaneous shift along the quasimomentum direction, $k_y \to k_y + \pi(2n+1)/q$ (here we use again that in the quasimomentum space k_y and $k_y + 2\pi$ are identified).

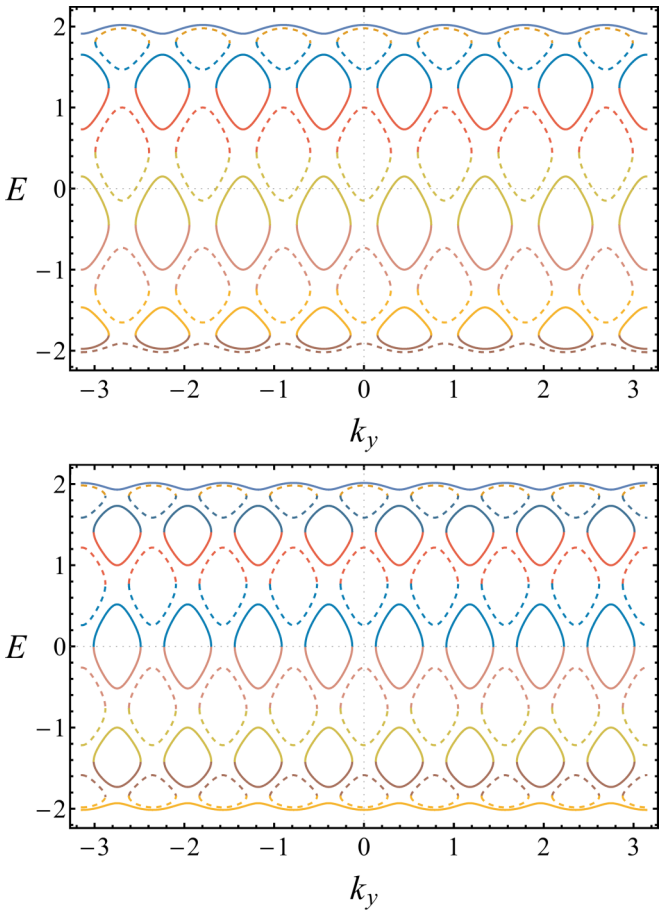

FIG. 2. (Color online) The energy spectrum E_q for odd $q = 7$ (top) and even $q = 8$ (bottom) as functions of the quasimomentum k_y for periodic (solid lines) and antiperiodic (dashed lines) boundary conditions on the x axis. The q energy branches are marked by different colors.

For even q, in the periodic case, both the highest and the lowest real energy levels are continuous curves for the whole interval $k_y \in [-\pi,\pi]$. The other $q-2$ branches are real only in q distinct k_y intervals. The $q-2$ energy branches are grouped pairwise to form $(q-2)/2$ distorted ovals in each of these intervals. Thus one has two continuous energy bands and $q(q-2)/2$ distorted energy ovals [see in Fig. 2 (bottom) the 24 solid ovals for $q = 8$]. The antiperiodic case is a bit simpler since the q energy branches are grouped pairwise to make $q/2$ separate energy ovals in the q bands. Thus one has $q^2/2$ distorted energy ovals [see Fig. 2 (bottom), the 32 dashed ovals for $q = 8$].

The symmetries of the even-q spectrum are simpler:

$$E^{(\pm)}_{q,r}(k_y)\Big|_{q\in\text{even}} = E^{(\pm)}_{q,r}(-k_y) = -E^{(\pm)}_{q,r}(k_y) = E^{(\pm)}_{q,r}\left(k_y + \frac{2\pi n}{q}\right), \tag{12}$$

with $n \in \mathbb{Z}$. The spectrum is symmetric with respect to mirroring of both energy $E \to -E$ and quasimomentum $k_y \to -k_y$. The spectrum is also invariant under the discrete shifts of the momenta, $k_y \to k_y + 2\pi n/q$. Contrary to q odd, for q even the energy spectra for periodic and antiperiodic boundary conditions are not simply related.

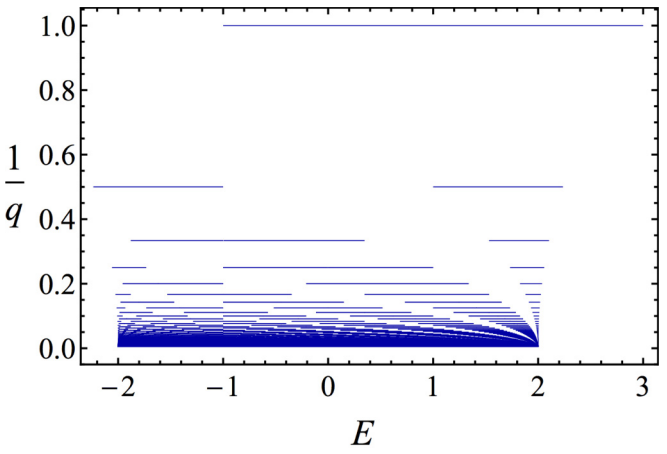

FIG. 3. (Color online) The band energy spectrum (the horizontal axis) with respect to the minimal value of the normalized magnetic flux $\beta = 1/q \in [0,1]$ with $q = 1,2,\ldots,100$ (the vertical axis) for periodic boundary conditions.

Finally, due to the independence of the spectrum on the numerator p of the (normalized) rational magnetic flux β in (3), the spectra in Fig. 2 (top) (bottom) are realized, in fact, for six different values of $\beta = p/7$ with $p = 1,\ldots,6$.

As can be clearly seen in Fig. 2, the real spectrum occupies the domain $[-\pi,\pi] \otimes [-2,2]$ with energy bands depending on the magnetic flux β. Following Ref. [3], we plot in Fig. 3 the energy bands as a function of $\beta = 1/q$ for $q = 1,2,\ldots,100$. Notice that the band spectrum does not carry any information on the actual quasimomentum dependence since it is obtained by a one-dimensional (1D) projection of the spectrum on the vertical (energy) axis. In the next section, we are going to show that not only the β dependence of the band spectrum but also the quasimomentum k_y dependence of the energy spectrum (9) have fractal self-similar patterns.

III. STRUCTURE OF ENERGY LEVELS

A. Structure of energy bands

It is well known that the Hofstadter band spectrum[2] $E \in [-4,4]$ reveals a fascinating fractal structure—the Hofstadter butterfly—when it is plotted on the horizontal axis against the normalized magnetic flux $\beta \in [0,1]$ on the vertical axis. Likewise, in the biased quantum model, a fractal structure should also materialize when the energy bands are plotted against β.

In Fig. 4, the band spectrum is plotted against β with all values $p/q \in [0,1]$ (and not only the minimal values $1/q$ as in Fig. 3) for $q = 1,\ldots,70$, both for periodic and antiperiodic boundary conditions. Here q plays the role of a "resolution" parameter that determines the thinness of the chosen grid of possible β values.

[2]Notice that in the biased quantum model, the real-valued band spectrum lies in the narrower interval $E \in [-3,3]$.

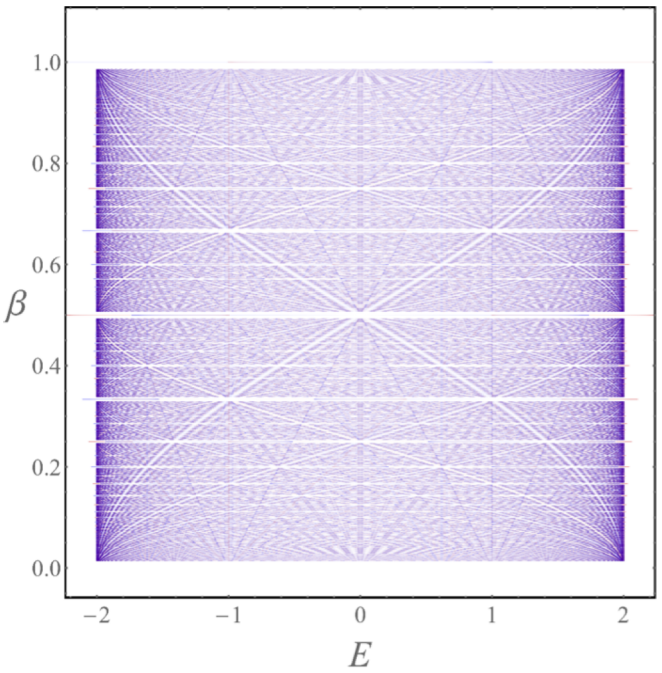

FIG. 4. (Color online) The band energy spectrum (the horizontal axis) with respect to the value of the normalized magnetic flux $\beta = p/q \in [0,1]$ with $q = 1,2,\ldots,70$ and $p = 1,\ldots,q$ (the vertical axis) for the periodic (the red lines) and antiperiodic (the blue lines) boundary conditions. The darkness (lightness) of the lines visualize high (low) values of the density of states (13).

In Fig. 4, the variations of lightness in each energy band correspond to the variations of the (normalized) density of states at a given energy,

$$\frac{1}{2\pi}\frac{dk_y}{dE}, \tag{13}$$

such that the higher (lower) the density of states is, the darker (lighter) is the band. As an illustration, in Fig. 5 (top and bottom) we display the density of states (13) and the corresponding energy levels for $q = 2,4,8$, respectively.

At a fixed resolution q, the (normalized) magnetic flux runs over the values

$$\beta = 0, \frac{1}{q}, \frac{2}{q}, \ldots, \frac{q-1}{q}, \tag{14}$$

where $\beta = 0$ corresponds to $p = q$. The energy levels are defined by Eqs. (7) and (8), i.e.,

$$\prod_{r=1}^{q}[E - 2\cos(k_y + 2\pi\beta r)] = e^{iqk_x}. \tag{15}$$

Evidently, some of the instances of p and q in Eq. (14) correspond to mutually reducible integers so that their greatest common divisor $\gcd(p,q) \neq 1$. In this case, one can use the property of the energy polynomial (8) that appears on the left-hand side of Eq. (15),

$$\prod_{r=1}^{q}[E - 2\cos(k_y + 2\pi\beta r)]\Big|_{\beta=\frac{p}{q}} = Q^{\gcd(p,q)}_{q/\gcd(p,q)}(E,k_y), \tag{16}$$

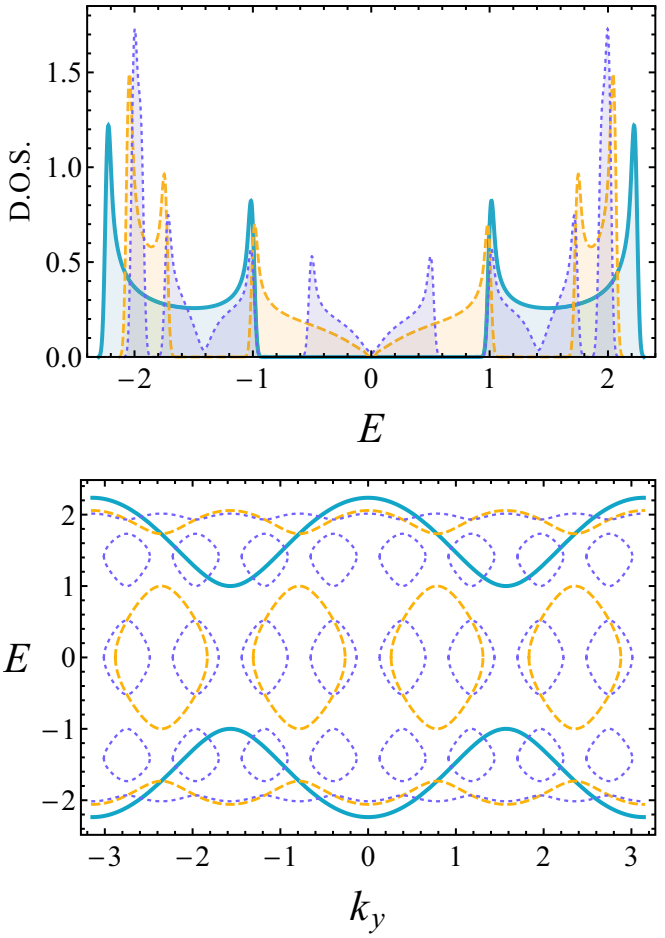

FIG. 5. (Color online) Top: the density of states (13) as a function of the energy E for $q = 2$ (the blue solid line), $q = 4$ (the orange long-dashed line), and $q = 8$ (the violet short-dashed line) levels. Bottom: the energy levels as a function of the quasimomentum k_y.

where

$$Q_q(E,k_y) = 2[T_q(E/2) - \cos(qk_y)], \tag{17}$$

and $T_q(x)$ is a Chebyshev polynomial of the first kind.[3]

Substituting Eq. (16) into Eq. (15), we get for the energy levels

$$Q^{\gcd(p,q)}_{q/\gcd(p,q)}(E,k_y) = e^{iqk_x}, \tag{18}$$

which can be simplified as

$$Q_{q_p}(E,k_y) = e^{iq_pk_x}, \tag{19}$$

where the integer q_p is

$$q_p = \frac{q}{\gcd(p,q)}. \tag{20}$$

We come to some trivial conclusions for the spectrum in the case of the rational (normalized) magnetic flux (5):

[3]We use the standard notation T_n for the Chebyshev polynomial of the first kind determined by the equation $T_n(\cos\varphi) = \cos(n\varphi)$.

(i) If p and q are mutual prime integers as in (6), then the energy spectrum is determined by

$$Q_q(E,k_y) = e^{iqk_x}, \tag{21}$$

because $q_1 \equiv q$.

(ii) If p and q are not mutual primes [$\gcd(p,q) \neq 1$], then the energy spectrum is determined by

$$Q_{q_p}(E,k_y) = e^{iqk_x}, \tag{22}$$

with q_p given in Eq. (20).

(iii) In the special case $p = q$, in which the magnetic field is absent, $\beta = 0$, we get the simple q-independent solution

$$E_{1,1}(k_y) = 2\left[\cos(k_y) + \frac{e^{ik_x}}{2}\right], \tag{23}$$

which is Eq. (9) for $q = 1$ and thus $r = 1$.

For $p = 1,2,\ldots,q-1$ the integer q_p runs over all possible divisors of the natural number q. Therefore, the nontrivial energy levels at resolution q are determined by Eq. (22), where the q_p's are taken from the set of all nonequal divisors of q.

For example, the scan of nonzero possible normalized magnetic fluxes with resolution $q = 6$ includes the series $\beta = 1/6,\ldots,5/6$. According to our discussion, the mutually prime numbers in $\beta = 1/6, 5/6$ share the common spectrum corresponding to $\beta = 1/6$, while $\beta = 2/6$ and $4/6$ correspond to the spectrum of $\beta = 1/3$ and $\beta = 3/6$ corresponds to the spectrum of $\beta = 1/2$. Therefore, the magnetic fluxes at resolution $q = 6$ should include the solutions at $\beta = 1/2,1/3,1/6$ [plus, of course, the trivial solution (23)]. In other words, the solutions are given by Eq. (9) with $q = 1,2,3,6$.

As yet another example, consider the magnetic fluxes with resolution $q = 16$, given by $\beta = 1/16,\ldots,15/16$, which can be divided into four different groups. The first group with the mutually prime numbers, $\beta = (2n+1)/16$, $n = 0,1,\ldots,7$, has a spectrum corresponding to the minimal representative $\beta = 1/16$. The second group, given by $\beta = 2(2n+1)/16$ with $n = 0,\ldots,3$, corresponds to the mutually prime numbers $\beta = (2n+1)/8$ with the minimal representative $\beta = 1/8$. The third group is $\beta = 4/16,12/16$, which has the same spectrum as $\beta = 1/4$. Finally, the last group includes only $\beta = 8/16 = 1/2$. Thus, the magnetic fluxes at resolution $q = 16$ should include the solutions corresponding to $\beta = 1/2,1/4,1/8,1/16$ and (23). In other words, the solutions are given by Eq. (9) in which $q = 1,2,4,8,16$ runs over the set of all divisors of 16.

Both examples illustrate that the energy levels with resolution q are given by the energy solutions (9) in which q_p runs over all possible divisors of the original resolution factor q [including, of course, the trivial energy level Eq. (23)]. The energy bands are plotted in Fig. 4: they have a characteristic pattern that no longer resembles a butterfly but rather a spider web.

B. Fractal energy levels in quasimomentum space

1. Self-similarity

To address the fractal structure of the eigenenergies of the non-Hermitian Hofstadter Hamiltonian (1) plotted as a function of the quasimomentum k_y, one has to consider curves made of all the disjoints energy ovals lying in the planar domain $[-\pi,\pi] \otimes [-3,3]$.

Let us focus on the series $q = m^n$ where the base m includes any integer $2,3,5,6,7,10,\ldots$ that is not a member of another series with a smaller base (i.e., $m \neq m_1^{n_1}$ for any integers $m_1 > 1$ and $n_1 > 1$). For example, Fig. 2 (top) for $q = 7$ is the starting plot of the series $q = 7^n$ with base $m = 7$, whereas Fig. 2 (bottom) for $q = 8$ belongs to the $m = 2$ series $q = 2 \to 4 \to 8 \to 16 \to 32 \to \cdots$. We are going to argue that for a given base m in the limit $n \to \infty$, the curve made of the reunion of all the disjoint ovals in each of the $q = m^n$ members of the series constitutes a fractal area-filling curve with Hausdorff dimension 2, as is the case for well-known area-filling curves such as, for example, the Peano, Wunderlich, or Hilbert curves [2].

The curves for the series $q = m^n$ with $m = 2,3,5$ are shown in Fig. 6. Note that they are not *per se* strictly self-similar because of the distortion of the ovals near the upper and lower energies $E = \pm 2$. Leaving aside these spurious boundary effects, the overall pattern is that of a fractal that remains unchanged by an increasingly accurate zooming. In the sequel, we concentrate on the central part of the energy plot, say $E \in [-1,1]$, where boundary effects become negligible and the self-similar structure of the oval patterns is manifest. As an example, the self-similarity of the energy levels in the $q = 2^n$ series is explicitly illustrated in Fig. 7. It is clear that in the central region (far from the distorted boundaries), the $q = 2^{n+1}$ energy levels are self-similar to a zoomed version of the $q = 2^n$ levels for any power n. This self-similarity depends on the base number m of the $q = m^n$ series. Thus, in the limit $n \to \infty$, we have not one but rather an infinite number of fractals labeled by the base m that one considers.

2. Energy levels as space-filling curves

There are several ways to determine the fractal structure of a 2D curve. One way is to consider a curve that, by successive iterations, would have a diverging length yet the area in which it is contained remains finite (typical examples of such curves are the Koch and Peano curves [2]). The scaling of the length of the curve with the length's resolution should give us the Hausdorff—fractal—dimension of the curve. Let us first address this question numerically, and then, in the next section, consider some more precise analytical arguments.

As we have already seen, at resolution q the number of energy ovals is $q(q-2)/2$ for an even q and $q(q-1)/2$ for an odd q. As a simple example, let us again consider the $q = 7$ and 8 curves of Fig. 2. Since the energy pattern repeats itself horizontally q times, it is sufficient to consider the part of the curve made of the ovals contained in a given k_y interval (a given column). Numerical estimates for $q = 2^n, q = 3^n, q = 5^n$, and large n (typically the maximal power is $n = 24$ for base $m = 2$) give for the perimeter length $\mathcal{L}^{\rm col}$ and the area enclosed $\mathcal{A}^{\rm col}$, respectively,

$$\mathcal{L}^{\rm col} = 7.347\,71, \quad \mathcal{A}^{\rm col} = \frac{7.748\,80}{q}. \tag{24}$$

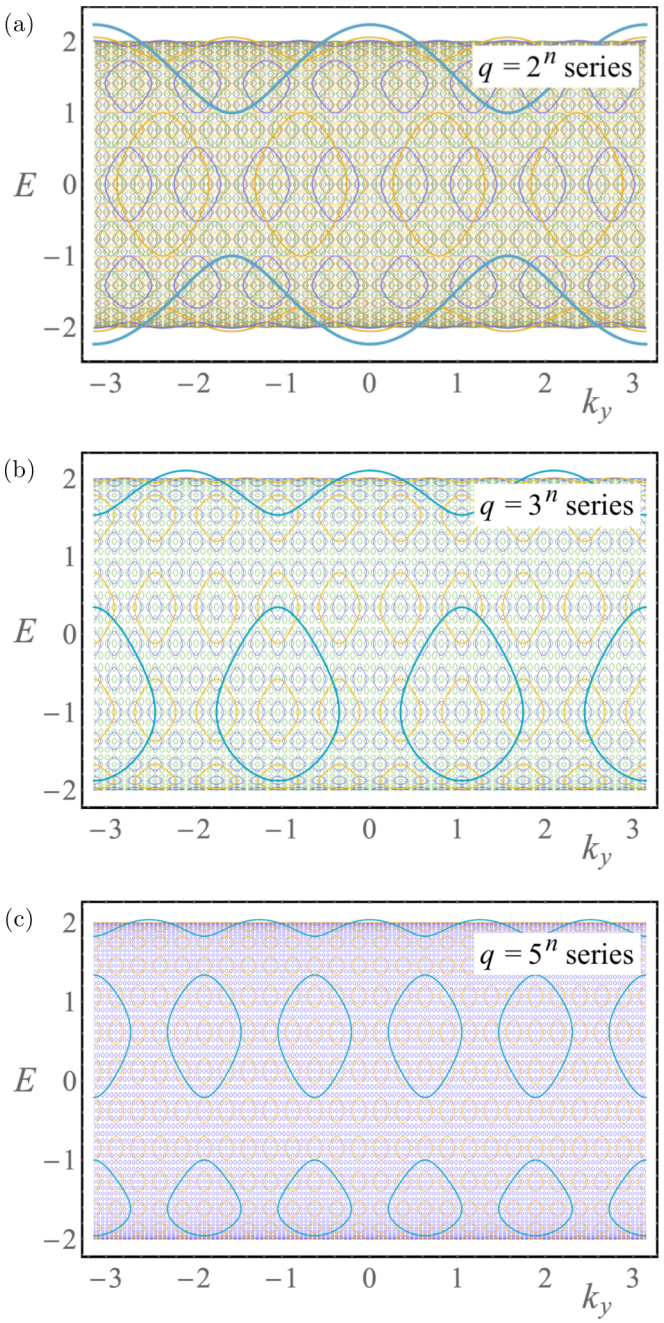

FIG. 6. (Color online) The energy spectra (9) are shown as functions of the quasi-momentum k_y at (normalized) magnetic fields $\beta = 1/q$ for $q = m^n$ series with (a) $m = 2$, $n = 1, \ldots, 6$; (b) $m = 3$, $n = 1, \ldots, 4$; (c) $m = 5$, $n = 1, \ldots, 3$.

As for the total perimeter length $\mathcal{L}^{\text{tot}}$ and the total area $\mathcal{A}^{\text{tot}}$ of the entire curve made of all the disjoint ovals, the scalings[4]

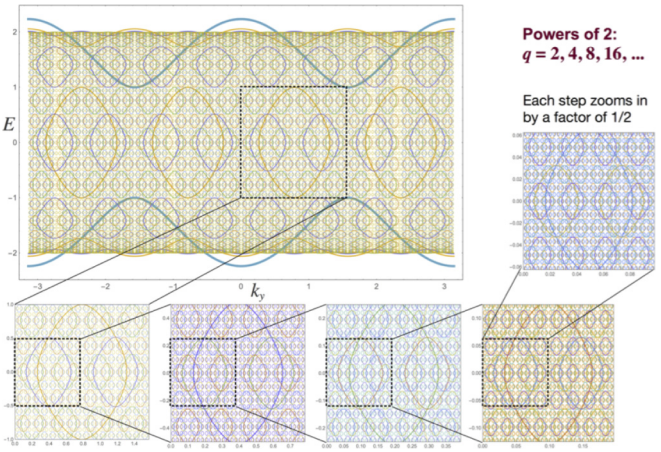

FIG. 7. (Color online) Zooming into the fractal structure of the energy levels of the non-Hermitian Hofstadter model for (normalized) magnetic fields $\beta = 1/q$ with $q = 2^n$ and increasing n.

are, respectively,

$$\mathcal{L}^{\text{tot}} \simeq 7.347\,71 \times q, \quad \mathcal{A}^{\text{tot}} \simeq 7.748\,80. \tag{25}$$

The scaling (25)—a diverging length for a curve that nevertheless encloses a finite area—is typical of a fractal area-filling curve. The Hausdorff dimension D of the curve and the resolution of the curve's details $1/q$—so that the bigger the resolution q, the smaller the scale at which one looks at the curve (as already mentioned, $1/q$ corresponds to the minimal possible nonzero value of the normalized magnetic flux β)—should be related by

$$\mathcal{L}^{\text{tot}} = \gamma \left(\frac{1}{q}\right)^{1-D}, \quad \mathcal{A}^{\text{tot}} = \text{const}. \tag{26}$$

A comparison of Eq. (25) with Eq. (26) gives a Hausdorff dimension $D = 2$, which corresponds to an area-filling curve.

Another way to show that the Hausdorff dimension is 2 consists in rephrasing the scaling argument above in terms of iterative patterns, which are clearly visible in Fig. 7 for base $m = 2$: each time the resolution is doubled, i.e., $1/q$ is divided by 2, the number of ovals is multiplied by 4. This property is again characteristic of a fractal with Hausdorff dimension $D = \ln 4/\ln 2 = 2$. In general for base m, iterating means dividing $1/q$ by m with a number of ovals multiplied by m^2, so again a Hausdorff dimension $D = \ln m^2/\ln m = 2$.

IV. CHEBYSHEV NESTING AND FRACTALS

The energy spectrum of the non-Hermitian Hamiltonian (1) is determined by Eqs. (17), (21), or (22), which involve Chebyshev polynomials of the first kind. The fractal structure of the $q = m^n$ series can surprisingly be understood in terms of the so-called "Chebyshev nesting," which is a composition identity for Chebyshev polynomials,

$$T_m[T_n(x)] = T_{mn}(x). \tag{27}$$

We can use three different approaches to discuss the relation of Chebyshev nesting (27) to the fractal self-similarity of the energy curves.

[4]Note that the area enclosed by the ovals is contained in a rectangle of area $2\pi \times 4 \simeq 25.1327$ whereas the "available" surface inside the rectangle, i.e., after removing the gaps between the bands, is [3] in the large q limit $2\pi \times 8/3 = 16.7552$.

First, let us consider the horizontal scaling of the energy solutions of Eq. (21). As we have already noticed in Figs. 2 and 6, the undistorted self-similar pattern of the energy levels is manifest in the vicinity of the $E = 0$ horizontal axis. The same self-similarity should be seen in particular in the scaling behavior of the zero-energy solutions that occur for a set of specific quasimomenta k_y. In other words, if, for the series $q = m^n$, the energy curves exhibit a self-similarity as the power n increases, then one might expect that the discrete quasimomenta k_y for which the energy lines cross the horizontal axis will also exhibit a self-similar scaling. According to Eqs. (17) and (21) for periodic boundary conditions—where indeed energy lines do cross the horizontal axis for both even and odd q—these zero-energy quasimomenta are given by

$$T_{m^n}(0) = \cos(m^n k_y) + \tfrac{1}{2}. \tag{28}$$

Using the Chebyshev nesting (27) as well as

$$T_q(0) = \cos\frac{\pi q}{2} \equiv \begin{cases} 0 & \text{for odd } q; \\ +1 & \text{for even } q, \quad \text{even } q/2; \\ -1 & \text{for even } q, \quad \text{odd } q/2 \end{cases} \tag{29}$$

and

$$T_q(+1) = +1, \quad T_q(-1) = (-1)^q, \tag{30}$$

one arrives at

$$T_{m^n}(0)\Big|_{n\geq 2} \equiv \underbrace{T_m(T_m(\cdots T_m(0)))}_{n\geq 2 \text{ times}} = f_m^+, \tag{31}$$

where

$$f_m^{\pm} = \frac{1 \pm (-1)^m}{2} \equiv \begin{cases} 1 & \text{even (odd) } m, \\ 0 & \text{otherwise.} \end{cases} \tag{32}$$

The important consequence of (27) is that, according to Eq. (31), $T_{m^n}(0)$ does not depend on n for $n \geq 2$. Then, in the periodic case at hand, the zero-energy quasimomenta solutions of Eq. (28) are

$$k_y^{(m,n,l)}(E = 0) = \frac{\pi}{6}\frac{1}{m^n}[3 - (-1)^m + 12l], \tag{33}$$

where $l \in \mathbb{Z}$ labels the possible independent solutions contained in the interval $[-\pi, \pi]$.

According to Eq. (33), for any two fixed powers n and $n + p$ with $p \in \mathbb{Z}$, the zero-energy quasimomenta are related by

$$k_y^{(m,n+p,l)}(E = 0) = \frac{1}{m^p} k_y^{(m,n,l)}(E = 0). \tag{34}$$

This implies that the zero-energy quasimomenta for $q = m^{n+1}$ can be obtained by a rescaling of the $q = m^n$ quasimomenta by a factor $1/m$. In other words, the width of the ovals diminishes by $1/m$ with each step $n \to n + 1$.

Secondly, let us consider the vertical scaling of the energy ovals for periodic boundary conditions. This scaling can be determined in a similar way using a simple argument based on the Taylor expansion of Chebyshev polynomials. Indeed, let us determine from Eqs. (17) and (21) the spectrum in the region close to the $E = 0$ axis where the energy spectrum is undistorted. For a given $q = m^n$, the Chebyshev polynomial in Eq. (17) can be expanded in power series as

$$T_{m^n}(x) = g_{m,n}(m^n x) + O\big(x^3\big), \tag{35}$$

where

$$g_{m,n}(y) = f_m^+ + f_m^-\big[f^+_{\frac{m-1}{2}} + (-1)^n f^-_{\frac{m-1}{2}}\big]y - \frac{f_m^+}{2}y^2. \tag{36}$$

The first two terms in the small-x expansion (35) depend solely on $m^n x$. The next-order term x^3 in Eq. (35) does not share the same scaling, but in the small energy region (or, equivalently, small x) it can be neglected, as can the higher-order terms. These facts play an important role for the fractal properties of the energy spectrum: indeed, keeping only these lowest-order terms, $g_{m,n}$ is invariant with respect to the shift $n \to n + 2$,

$$g_{m,n+2}(y) = g_{m,n}(y). \tag{37}$$

One can then distinguish two sectors according to the parity of n,

$$g_m^{\text{even}}(y) \equiv g_{m,n}(y)\big|_{n\in\text{even}} = f_m^+ + f_m^- y - \frac{f_m^+}{2}y^2, \tag{38}$$

$$g_m^{\text{odd}}(y) \equiv g_{m,n}(y)\big|_{n\in\text{odd}} = f_m^+ + y\sin\frac{\pi m}{2} - \frac{f_m^+}{2}y^2, \tag{39}$$

where $\ell_n =$ even (odd) for even (odd) n, respectively. For a given ℓ_n, $g_m^{\ell_n}$ is independent of n.

Clearly, for $q = m^n$ with periodic boundary conditions, the energy close to the horizontal axis is determined by

$$g_m^{\ell_n}\left(\frac{m^n E}{2}\right) = \cos(m^n k_y) + \frac{1}{2}. \tag{40}$$

Due to the independence on n on the left-hand side of Eq. (40), once the parity ℓ_n is fixed, the energy solutions for $q = m^{n+2p}$ and $q = m^n$ are related by

$$E^{(m,n+2p)}(k_y) = m^{-2p} E^{(m,n)}(m^{2p} k_y), \tag{41}$$

where $p \in \mathbb{N}$ is an arbitrary natural number. The self-similar scaling property (41) is consistent with the zero-energy quasimomenta scaling (34).

The explicit solutions of Eqs. (38), (39), and (40),

$$E^{(m,n)} = \begin{cases} \pm\frac{\sqrt{1-2\cos(m^n k_y)}}{m^n} & \text{even } m, \\ \frac{1+2\cos(m^n k_y)}{m^n}(-1)^{\frac{(m-1)n}{2}} & \text{odd } m, \end{cases} \tag{42}$$

are low-energy solutions valid in the region $m^n|E| \ll \pi$. They highlight the self-similarity properties (34) and (41) of the energy spectrum as n increases.

Thirdly, there is a slightly more elegant and general way to show the fractal self-similarity of the spectrum both for periodic and antiperiodic boundary conditions by using yet another property of the Chebyshev polynomials,

$$\lim_{n\to\infty}[(-1)^{mn} T_{m^n}(m^{-n}x)] = \begin{cases} \cos x, & \text{even } m, \\ \sin x, & \text{odd } m. \end{cases} \tag{43}$$

For practical purposes, it is convenient to use an approximate formula based on (43),

$$T_{m^n}(m^{-n}x) \to T^{(0)}_{m^n}(m^{-n}x) = f^+_m \cos x + (-1)^{mn} f^-_m \sin x, \tag{44}$$

where $f^\pm_m$ is given in Eq. (32). The approximation made in (44) is valid in the interval $x \in [-\pi,\pi]$ with an error 10^{-4} for $m = 2, n = 4$. The accuracy of this approximation is increasing rapidly as either m or n or both become larger (for example, for $m = n = 4$ the error is less than 10^{-8}).

For large n one can combine, both for periodic and antiperiodic boundary conditions, Eqs. (17), (21), and (44) into

$$\begin{aligned} \text{even } m: \quad & \cos\frac{m^n E}{2} = \cos(m^n k_y) \pm \frac{1}{2}, \\ \text{odd } m: \quad & (-1)^n \sin\frac{m^n E}{2} = \cos(m^n k_y) \pm \frac{1}{2}, \end{aligned} \tag{45}$$

which are again valid in the energy domain $m^n|E| \ll \pi$. One can check that the solutions of Eqs. (45) reproduce the lowest energy levels.

The symmetries of Eqs. (45) clearly imply the fractal self-similarity of the energy levels,

$$E^{(m,n+p)}(k_y) = (-1)^{mp} m^{-p} E^{(m,n)}(m^p k_y), \tag{46}$$

both for even and odd m and $p \in \mathbb{N}$. These equations are consistent with the scalings (34) and (41).

Equation (46) implies that the energy spectrum for $q = m^{n+1}$ can be obtained by the following:

(i) Rescaling (i.e., squeezing) the $q = m^n$ solution by the factor $1/m$ both in the energy E and quasimomentum k_y coordinates.

(ii) Periodically copying (i.e., extending) the squeezed solution m times along the energy E axis and m times along the quasimomentum k_y axis.

Note that these properties cannot be readily seen from the original Eq. (9). They highlight three important properties of the $q = m^n$ series, which were already numerically illustrated above. As $n \to n+1$:

(a) The total area $\mathcal{A}_n$ enclosed by the energy ovals in a fixed *area* of the (k_y, E) plane remains constant since the ovals become m times smaller in each of the two (k_y and E) directions while their number increases by a factor m^2 so that $\mathcal{A}_{n+1} = \mathcal{A}_n$.

(b) The total lengths $\mathcal{L}^{\rm col}_n$ and $\mathcal{L}^{\rm row}_n$ of the energy oval perimeters in a fixed *column* and a fixed *row*, respectively, remain constant since they become m times smaller while their numbers in each column and in each row increase by a factor m so that $\mathcal{L}^{\rm col}_{n+1} = \mathcal{L}^{\rm col}_n$ and $\mathcal{L}^{\rm row}_{n+1} = \mathcal{L}^{\rm row}_n$.

(c) The total length of the energy oval perimeters $\mathcal{L}^{\rm tot}_n$ in a fixed *area* in the (k_y, E) plane increases by a factor m so that $\mathcal{L}^{\rm tot}_{n+1} = m\mathcal{L}^{\rm tot}_n$ due to the second property as well as because the number of columns and ovals increases by the same factor m.

When $n \to \infty$, these three properties imply that the total length of the energy curves (i.e., of the oval perimeters) in a fixed area of the (k_y, E) plane diverges as $\mathcal{L}^{\rm tot}_n \propto m^n$ while the area $\mathcal{A}$ enclosed by these ovals remains constant. Thus, a union of the energy ovals indeed constitutes an area-filling curve with Hausdorff dimension $D = 2$. In agreement with Eq. (26), the size $a_n \propto 1/q \equiv 1/m^n$ of any individual oval along any direction decreases with an increasing resolution, $q \to \infty$, so that one gets $\mathcal{L}^{\rm tot}_n \propto a_n^{-1} \equiv a_n^{1-D}$ with the usual $D = 2$ Hausdorff dimension for space-filling curves.

Notice that the band structure of the energy levels has been obtained by projecting the k_y-dependent energy levels on the vertical energy axis and plotting it against the magnetic flux β. Since the quasimomentum-dependent energy levels are self-similar, we conclude that for a fixed base m the energy band spectrum must also exhibit a fractal self-similarity for the different powers n of the normalized magnetic flux $\beta = 1/m^n$, as illustrated in Fig. 4.

V. FLATTENED ENERGY SPECTRA

A. Flattening

The fractal self-similarity of the real-valued energy spectrum (9) can be addressed in yet another way. As stressed above, the energy ovals are distorted near both edges of the spectrum $E \sim \pm 2$ (as illustrated in Fig. 6). On the other hand, in the center $E \sim 0$, the distortion is practically absent and the self-similarity is quite pronounced. It turns out that in order to remove the boundary distortion effects from the entire energy domain, it is sufficient to consider, instead of the energy itself, the energy-related quantity

$$\mathcal{E}_{q,r}(k_y) = \arccos\left[\frac{1}{2}E_{q,r}(k_y)\right] \tag{47}$$

in the interval $\mathcal{E} \in [0,\pi]$.

Using (9) for the q energy branches $r = 1, \ldots, q$ of the original spectrum, one can rewrite Eq. (47) as

$$\mathcal{E}_{q,r}(k_y) = f\left[\frac{1}{q}\left(\arccos\left[\cos(qk_y) + \frac{e^{iqk_x}}{2}\right] + 2\pi r\right)\right], \tag{48}$$

where

$$f(x)\Big|_{x\in[0,2\pi]} = \pi - |x - \pi| \equiv \arccos(\cos x). \tag{49}$$

The flattened spectra (47) are shown in Fig. 8(a), 8(b), and 8(c), respectively, for the $q = m^n$ series with $m = 2$, 3, and 5—they correspond to the unflattened spectra of Fig. 6. Clearly, the arccos operator in Eq. (47) "unfolds" the spectrum by flattening the energy levels close to $E = \pm 2$, so that no distortion is present anymore. It follows that the fractal self-similarity of the spectrum is manifest in the whole energy domain.

For example, in Fig. 8(a), each of the $q = 2^n$ energy ovals intersects with two smaller $q = 2^{n+1}$ energy ovals for $n = 1, \ldots, 5$. Analogously in Fig. 8(b), each of the $q = 3^n$ energy ovals intersects with four and includes one smaller $q = 3^{n+1}$ energy oval for $n = 1, \ldots, 3$. And in Fig. 8(c), a similar self-similarity pattern can easily be observed for the $q = 5^n$ series.

B. Self-similarity for the flattened bands

In addition to these visual observations, one can make a more precise statement on the self-similarity. In Fig. 9, we plot the flattened band spectra for $q = m^n$ with $m = 2, 3, 5$. These plots share certain features with Fig. 3 but with the difference

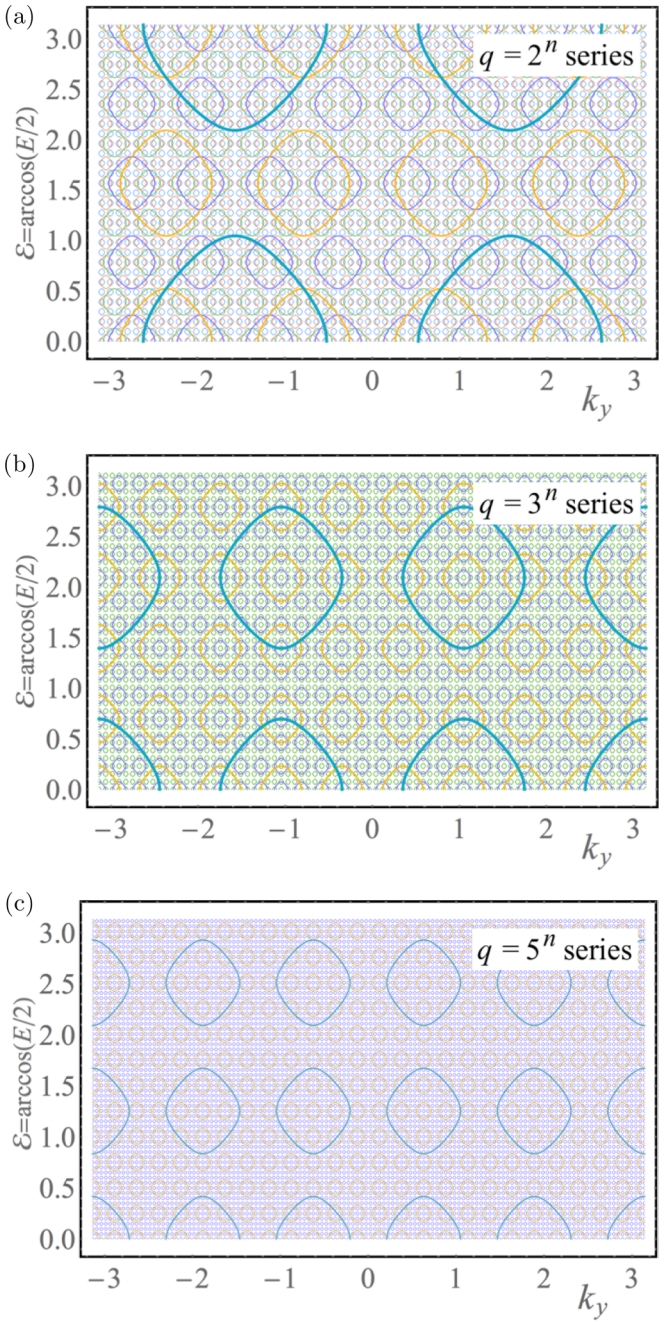

FIG. 8. (Color online) The flattened energy spectra (47) vs the quasimomentum k_y for $q = m^n$ series with (a) $m = 2$, $n = 1,\ldots,6$; (b) $m = 3$, $n = 1,\ldots,4$; and (c) $m = 5$, $n = 1,\ldots,3$. These plots correspond the original energy spectra shown in Fig. 6.

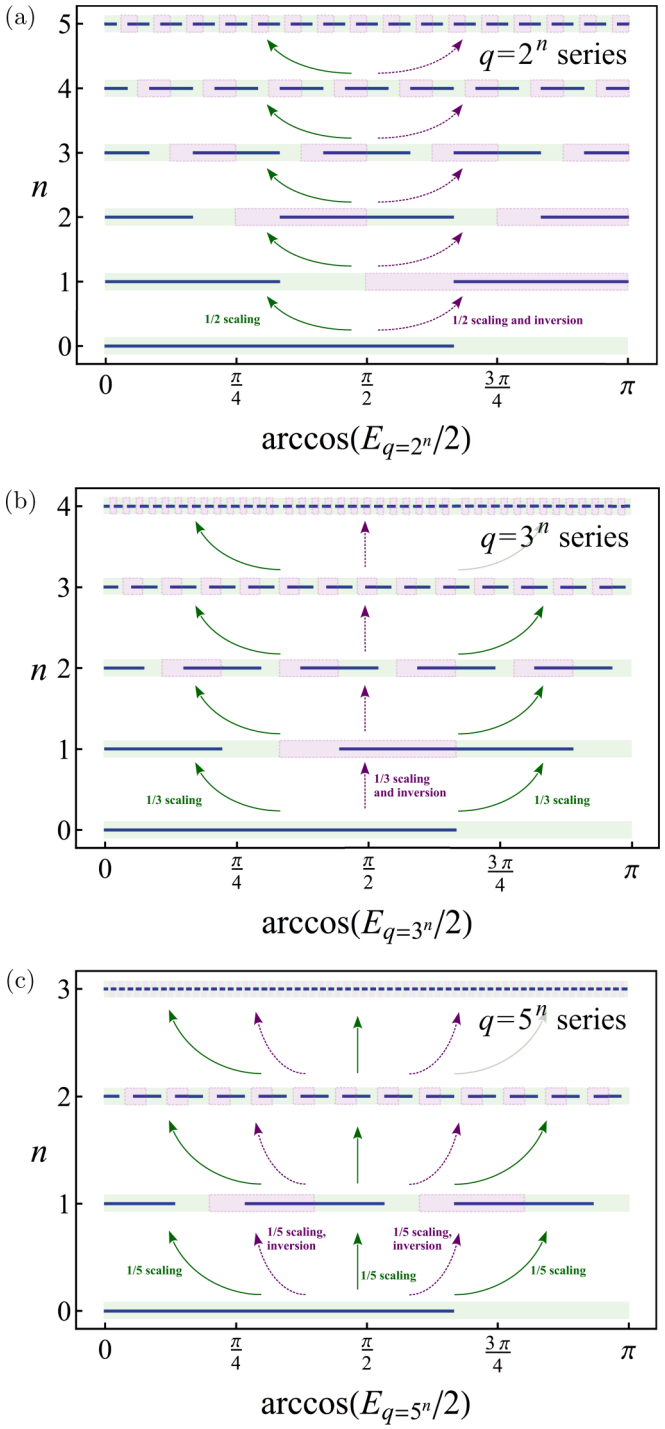

FIG. 9. (Color online) The blue horizontal lines: The arccosine (47) of the energy levels (9) for the series $q = m^n$ at fixed power n and for (a) $m = 2$, (b) $m = 3$, and (c) $m = 5$. The shadowed regions and the arrows show the self-similarity features.

being that in Fig. 9 the vertical axis shows the power n for a given base m instead of $1/q$ for a set of q's.

Consider first in Fig. 9(a) the $q = 2^n$ series. The spectrum at the lowest level $n = 0$ has—in terms of the flattened energy variable (47)—a single band of width $\delta\mathcal{E}_{2^0} = 2\pi/3$ and a gap of width $\pi/3$. To get the spectrum at the next level $n = 1$, it is sufficient to do the following:

(i) Rescale the original $n = 0$ spectrum, shrinking it by a factor $1/2$ so that $\mathcal{E} \in [0,\pi] \to \mathcal{E} \in [0,\pi/2]$.

(ii) Duplicate the resulting spectrum to cover again the whole energy range, $\mathcal{E} \in [0,\pi/2] \cup [\pi/2,\pi] \to \mathcal{E} \in [0,\pi]$.

(iii) Finally, invert the duplicate around its center $\mathcal{E} = 3\pi/4$.

Obviously, the total width of the two resulting bands at level $n = 1$ remains equal to the width of the single original $n = 0$ band, $\delta\mathcal{E}^{\rm tot}_{2^1} = \delta\mathcal{E}_{2^0}$.

Recursively, the band spectrum at level $n+1$ is obtained by applying the same rescaling-duplicating-inverting procedure on the spectrum at level n:

(i) Rescale the spectrum by a $(1/2)$ shrinking.

(ii) Duplicate the resulting spectrum.

(iii) Invert the duplicate around its center $\mathcal{E} = 3\pi/4$.

In Fig. 9(a), this procedure is explicitly illustrated up to level $n = 5$. Note that some pairs of adjacent smaller bands merge into single bands that are twice as wide. Note also that the inversion is not trivial only for the first iteration $n = 0 \to n = 1$ since from $n = 1$ onward the spectrum becomes symmetric around its center.

As a result, for the $q = 2^n$ series, at level $n \geqslant 1$ there are $(2^n + 2)/2$ bands with individual widths necessarily summing to

$$\delta\mathcal{E}^{\rm tot}_{2^n} = \frac{2\pi}{3}. \tag{50}$$

By construction, this band spectrum is evidently self-similar, and it becomes a fractal in the limit $n \to \infty$.

Likewise, consider in Fig. 9(b) the flattened energy bands for the series $q = 3^n$ up to level $n = 4$. Starting from level n, the iterative procedure consists in the following:

(i) Rescaling the spectrum by a $(1/3)$ shrinking.

(ii) Triplicating the resulting spectrum.

(iii) Finally, inverting the second copy around its center $\mathcal{E} = \pi/2$.

Once again, pairs of adjacent bands merge into single bands that are twice as wide. As a result, for the $q = 3^n$ series, at level $n \geqslant 1$ there are $(3^n + 1)/2$ bands that again have a total width $\delta\mathcal{E}^{\rm tot}_{3^n} = 2\pi/3$, as in Eq. (50). Similar to the $q = 2^n$ series, in the limit $n \to \infty$ the $q = 3^n$ band spectrum becomes a fractal.

A similar iterative procedure applies to the band spectrum for the $q = 5^n$ series as illustrated in Fig. 9(c) up to level $n = 3$. The bands at level $n+1$ are constructed from the bands at level n by a $1/5$-shrinking, 5-plicating, and inversion of every even copy around their centers $\mathcal{E} = 3\pi/10$ and $\mathcal{E} = 7\pi/10$, respectively. Again adjacent bands merge into single bands that are twice as wide so that at level $n \geqslant 1$ there are $(5^n + 1)/2$ bands with a total width $\delta\mathcal{E}^{\rm tot}_{5^n} = 2\pi/3$. Clearly, in the limit $n \to \infty$ the $q = 5^n$ spectrum becomes a fractal.

The universality of the iterative self-similar procedure is now evident. For the $q = m^n$ series, the band spectrum at level $n+1$ can be constructed from the band spectrum at level n by (i) $(1/m)$ shrinking, (ii) m-plicating, and (iii) inverting every even copy around their centers $\mathcal{E} = (2k-1)\pi/(2m)$ with $k = 2,4,\ldots$.

As a result, at level $n \geqslant 1$ there are $(m^n + 1)/2$ (for odd m) or $(m^n + 2)/2$ (for even m) bands with a total width $\delta\mathcal{E}^{\rm tot}_{m^n} = 2\pi/3$. This implies that the bands always occupy $2/3$ of the available flattened energy range $[0,\pi]$. The universality of the procedure is highlighted by the fact that all the band spectra are constructed from the same initial $n = 0$ level band spectrum.

For every given base m, each successive iteration $n \to n+1$ has the bands shrinking to smaller bands. Thus, in the limit $n \to \infty$, one obtains a pointlike spectrum consisting of infinitely many bands of infinitely small width. The structure of the band spectrum is similar to a Cantor set with a difference, which is, however, essential: contrary to the Cantor set, the total bandwidth is the nonzero base-independent quantity

$$\lim_{n\to\infty} \delta\mathcal{E}^{\rm tot}_{m^n} = \frac{2\pi}{3}. \tag{51}$$

Thus, similarly to the original unflattened band spectrum, the flattened band spectrum has a fractal self-similar structure when plotted against the normalized magnetic flux $\beta = p/q$ with $p = 1,\ldots,q$, with a resolution $q = m^n$ for base m determined by the increasing level number n. The self-similarity pattern depends on m, but the total bandwidth (51) is m-independent. The flattened band spectrum has a Hausdorff dimension $D = 1$ that follows from the $1/m$-shrinking m-plicating iterative procedure.

Finally, we stress that, as far as the unflattened spectrum $E(k_y)$ in Eq. (9) is concerned, distortion effects tend to disappear in the $n \to \infty$ limit: as n increases, the energy "ovals" distortion effects migrate from the center of the spectrum $E \sim 0$ toward its edges, $E \to \pm 2$. In other words, in the limit of an infinitely large $q = m^n$ resolution, regions with distorted ovals eventually disappear at the edges of the energy domain. This feature is clearly visible in the plots of Fig. 6, which are worth comparing with their corresponding flattened versions in Fig. 8. In Ref. [3], the unflattened $q \to \infty$ spectrum was shown to have a total bandwidth saturating to $8/3$. Compared to the total unflattened energy range, $E \in [-2,2]$, the bands therefore occupy in this limit $2/3$ of the whole energy interval. Equation (51), not surprisingly, leads to the same conclusion for the flattened band spectrum.

VI. COMPLEX ENERGY BRANCHES

So far we have discussed the real energy branches of the non-Hermitian Hamiltonian (1). However, the full spectrum contains energy branches with a nonzero imaginary part. Since these energies correspond either to some formal instabilities or to a dissipative motion of the particles, they are not particularly relevant for a large system at thermodynamic equilibrium. Still,

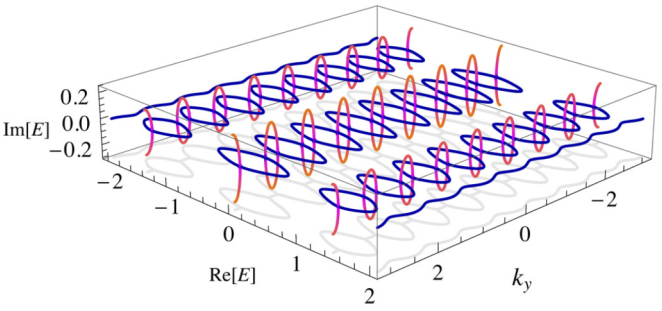

FIG. 10. (Color online) The real and imaginary parts of the energy spectrum for $q = 8$ plotted against the quasimomentum k_y. The horizontal blue lines represent the real spectrum ($\mathrm{Im}E = 0$) while the vertical red-orange lines correspond to the complex spectrum with a nonzero imaginary part ($\mathrm{Im}E \neq 0$). A projection of the energy spectrum on the bottom of the plot is also presented for convenience (gray color).

for the sake of completeness, we find it appropriate to display the entire spectrum with its complex energy modes.

In Fig. 10, the $q = 8$ spectrum is displayed in a 3D (k_y, ReE, ImE) plot. The real branches shown in Fig. 2 are recognizable in the horizontal (k_y, ReE, Im$E = 0$) plane. They build ordered chains of distorted ovals. Similarly, the complex branches build ordered chains of distorted ovals in the (k_y, Re$E = 0$, ImE) plane. These complex ("vertical" in the 3D plot) ovals connect the real ("horizontal") ovals in a 3D chainlike manner.

Energy spectra for generic q values, both for periodic and antiperiodic boundary conditions, are similar to Fig. 10, with horizontal real ovals always connected by vertical complex ovals along the k_y coordinate. This observation gives strong evidence to the fact that the entire energy spectrum—with the imaginary branches included—is also a fractal, similar to the real energy spectrum.

VII. DISCUSSION AND CONCLUSIONS

In our paper, we have studied the fractal properties of the energy spectrum of a charged particle with a biased motion on a two-dimensional square lattice in the background of a magnetic field. This biased quantum model is such that the particle is not allowed to hop in one of the directions (say, to the left) while it can freely move in all other directions. Its dynamics is described by a non-Hermitian Hamiltonian of a Hofstadter type.

It is worth mentioning that biased random walks arise in a wide range of systems in weakly off-equilibrium states, from chemotaxis in biology (when small living organisms, notably bacteria, are stimulated to randomly move with a biased preference toward a low gradient of a chemical solution in a liquid or gas—i.e., essentially, by a weakly space-dependent chemical potential—or by a temperature and/or pressure gradients) [5] to the directed diffusion of particles on fractal structures in the presence of an applied field [6]. In these examples, the biased motion should have a milder degree of bias compared to the limiting case considered here, so that the motion of a particle to a certain direction (say to the left, as in our case) should not be completely forbidden compared to the motion to another (say right) direction. This issue needs further investigation and we plan to address it in a forthcoming article. Possible applications of the non-Hermitian model (1) to real experimental systems—such as 2D electronic samples with a perpendicular magnetic field like in the quantum Hall effect—were discussed in the last section of Ref. [3] (see also [7] for a general discussion of non-Hermitian quantum-mechanical models).

Although at the moment we know no explicit examples of the biased motion of the electrons on a square lattice to which our work may directly apply, one might expect that the biased propagation may be realized in certain weakly nonequilibrium states of the mentioned system. Indeed, one may argue that most known examples of the biased random walks, such as chemotaxis [5] and directed diffusion [6], occur in slightly off-equilibrium states that are characterized either by a slow gradient of concentration of a certain chemical in a liquid or gas (i.e., essentially, by a weakly space-dependent chemical potential), or by temperature and/or pressure gradients.

In our article, we have shown that in the non-Hermitian Hamiltonian of a Hofstadter type, the corresponding energy spectrum, which depends on the normalized magnetic flux—the ratio of the magnetic flux threading an elementary plaquette to the magnetic flux quantum—possesses a nested multifractal structure.

The energy bands, plotted against the rational magnetic flux, exhibit a fractal pattern shown in Fig. 4. Contrary to Hofstadter's butterfly, the band spectrum is rather similar to a spider web.

The energy levels, plotted against the quasimomentum, exhibit even more curious fractal patterns as illustrated in Fig. 6. We have shown, both numerically and analytically, that the real energy spectrum is an overlap of infinitely many inequivalent fractals that we call "fractal energy carpets." The energy levels in each fractal are space-filling curves with Hausdorff dimensions 2.

In a more rigorous approach, we have shown that for a given base m and resolution $q = m^n$ with $n \in \mathbb{N}$, the energy curves for the normalized magnetic flux $\beta = 1/m^n$ ($m = 2,3,5,6,7,10, \ldots$ is required to not be equal to a natural power of a natural number) have a self-similar geometric structure. This self-similarity is observed up to certain finite scales, both in quasimomentum and in energy, constrained by the finiteness of n. In the limit of an infinitely fine resolution, $n \to \infty$, the structure of the energy level becomes a fractal with various fractal carpets depending on the base m considered.

We have also shown that the real branches of the energy spectrum are connected by complex branches forming chainlike structures in the 3D space of the energies plotted against the quasimomentum. The fractal properties of the energy levels are visualized in the supplementary video material [9].

ACKNOWLEDGMENT

The work of M.N.C. was partially supported by Far Eastern Federal University Grant No. 13-09-0617-m_a.

[1] D. R. Hofstadter, Energy levels and wave functions of Bloch electrons in rational and irrational magnetic fields, Phys. Rev. B **14**, 2239 (1976).

[2] B. Mandelbrot, *The Fractal Geometry of Nature* (Freeman, San Francisco, 1982).

[3] S. Matveenko and S. Ouvry, The area distribution of two-dimensional random walks and non Hermitian Hofstadter quantum mechanics, J. Phys. A **47**, 185001 (2014).

[4] S. Mashkevich and S. Ouvry, Area distribution of two-dimensional random walks on a square lattice, J. Stat. Phys. **137**, 71 (2009).

[5] M. Eisenbach *et al.*, *Chemotaxis* (Imperial College Press, London, 2004).

[6] S. Havlin, A. Bunde, H. E. Stanley, and D. Movshovitz, Diffusion on percolation clusters with a bias in topological space: Non-universal behavior, J. Phys. A **19**, L693 (1986); V. Balakrishnan and C. Van den Broeck, Transport properties on a random comb, Physica (Amsterdam) **217**, 1 (1995).

[7] C. M. Bender, Making sense of non-Hermitian Hamiltonians, Rep. Prog. Phys. **70**, 947 (2007).

[8] J. Zak, Magnetic translation group, Phys. Rev. **134**, A1602 (1964); Magnetic translation group. II. Irreducible representations, **134**, A1607 (1964).

[9] See Supplemental Material at http://link.aps.org/supplemental/10.1103/PhysRevE.92.042102 for a video visualizing the fractal properties of the energy levels.